energies

MDPI

Article

Emergency Pump-Rate Regulation to Mitigate Water-Hammer Effect—An Integrated Data-Driven Strategy and Case Studies

Lei Hou [1,*], Peibin Gong [2], Hai Sun [3], Lei Zhang [3,*], Jianhua Ren [4] and Yiyan Cheng [4]

[1] China-UK Low Carbon College, Shanghai Jiao Tong University, Shanghai 201306, China
[2] Drilling Technology Research Institute of SINOPEC, Shengli Oilfield Service Corporation, Dongying 257017, China
[3] School of Petroleum Engineering, China University of Petroleum (East China), Qingdao 266580, China
[4] Research Institute of Exploration & Development, East China Company of SINOPEC, Nanjing 210011, China
* Correspondence: leihou@sjtu.edu.cn (L.H.); zhlei@upc.edu.cn (L.Z.)

Abstract: Pump-rate regulation is frequently used during hydraulic fracturing operations in order to maintain the pressure within a safe range. An emergency pump-rate reduction or pump shutdown is usually applied under the condition of sand screen-out when advancing hydraulic fractures are blocked by injected proppant and develop wellhead overpressure. The drastic regulation of the pump rate induces water-hammer effects—hydraulic shocks—on the wellbore due to the impulsive pressure. This wellbore shock damages the well integrity and then increases the risk of material leakage into water resources or the atmosphere, depending on the magnitude of the impulsive pressure. Therefore, appropriate emergency pump-rate regulation can both secure the fracturing operation and enhance well-completion integrity for environmental requirements—a rare mutual benefit to both sides of the argument. Previous studies have revealed the tube vibration, severe stress concentration, and sand production induced by water-hammer effects in high-pressure wells during oil/gas production. However, the water-hammer effect, the induced impulsive pressures, and the mitigation measures are rarely reported for hydraulic fracturing injections. In this study, we present a data-driven workflow integrating real-time monitoring and regulation strategies, which is applied in four field cases under the emergency operation condition (screen-out or near screen-out). A stepwise pump-rate regulation strategy was deployed in the first three cases. The corresponding maximum impulsive pressure fell in the range of 3.7~7.4 MPa. Furthermore, a sand screen-out case, using a more radical regulation strategy, induced an impulsive pressure 2 or 3 times higher (~14.7 MPa) than the other three cases. Compared with the traditional method of sharp pump-rate regulation in fields, stepwise pump-rate regulation is recommended to constrain the water-hammer effect based on the evolution of impulsive pressures, which can be an essential operational strategy to secure hydraulic fracturing and well integrity, especially for fracturing geologically unstable formations (for instance, formations near faults).

Keywords: hydraulic fracturing; well integrity; pump rate; water hammer effect; case study

check for updates

Citation: Hou, L.; Gong, P.; Sun, H.; Zhang, L.; Ren, J.; Cheng, Y. Emergency Pump-Rate Regulation to Mitigate Water-Hammer Effect—An Integrated Data-Driven Strategy and Case Studies. *Energies* **2024**, *17*, 1157. https://doi.org/10.3390/en17051157

Academic Editors: Chongwei Xiao, Fatick Nath, Deepak Ganta and Zhiyang Li

Received: 3 January 2024
Revised: 18 January 2024
Accepted: 20 January 2024
Published: 29 February 2024

Copyright: © 2024 by the authors. Licensee MDPI, Basel, Switzerland. This article is an open access article distributed under the terms and conditions of the Creative Commons Attribution (CC BY) license (https://creativecommons.org/licenses/by/4.0/).

1. Introduction

The advent of massive hydraulic fracturing has spurred the shale gas revolution, but it has ignited controversy over unresolved environmental effects [1–3]. Scientists focused on the potential for water contamination soon after the adoption of the technique circa 2011 [4–6] and have continued to track the quality of aquifers ever since, especially in the shale-gas-producing regions across the United States [7–9]. Multiple lines of evidence (e.g., chemical and isotopic signatures) are reported to demonstrate the effects of stray gas contamination [10–13], while others present a counter perspective [14–16]. Over the same period, the rapid development of hydraulic fracturing occurred in the United States, China, and other energy-intensive economies. Recently, the U.S. DOE (Department of

Energy) released a presidentially mandated report concerning the economic and national security effects of any potential hydraulic fracturing ban [17], whilst the California state government, in the same year, announced a cessation in the issuing of new fracking permits after 2024 [18]. The disparity between the two sides of the debate seems to have resulted in an impasse. Based on the reality that massive wells are still fracked every year, the argument over whether to engage in fracking has overshadowed an urgent issue that has already caused significant economic losses and potential risks of material leakage as a result of dangerous screen-out incidents during hydraulic fracturing. Moreover, this joint mitigation of potential economic losses and of environmental contamination represents a rare case of an aligned, mutual interest for both parties in the conflict.

Initial efforts focused on detecting the migration of underground materials around fractured wells. Focused studies then noted that the key pathways were potential flaws in the casing and cement sheathing due to the quality of well completion and their routine failure during their service lives [5,16]. However, recent observations indicate that largely routine incidents (mainly sand screen-out) during fracturing also affect well integrity [19–21]. Sand screen-out often causes a sudden pressure jump that may exceed the capacity of the wellbore or wellhead equipment, which may deform the casing and compromise wellbore integrity [21]. An emergency pump-rate shut-down is usually performed to relieve the building pressure, which, in turn, may cause severe vibration and damage to the casing and cement annulus due to water-hammer effects [19,20]. These mechanical processes are graphically represented in Figure 1. Material leakages may occur through ① flaws between the cement and the casing, ②③ flaws and gaps between the cement and the formation, ④ cracked cement, and ⑤ deformed casing [5,22]. Thus, compromised wells can generate hyperchannels for the migration of underground materials. A significant breach in the casing may transmit pressure along the outer cement annulus and up to the above-ground wellhead. This has been observed as a common phenomenon in 30%~66% of fractured wells in the Changning–Weiyuan and Weirong areas of the Sichuan Basin, China [21,23], and in 6.3% (more than 500 wells) of fractured wells between 2005 and 2013 in the Marcellus shale in the United States [24]. Less perceptible damage may be manifest as late failures and risks to the environment over the well's lifetime.

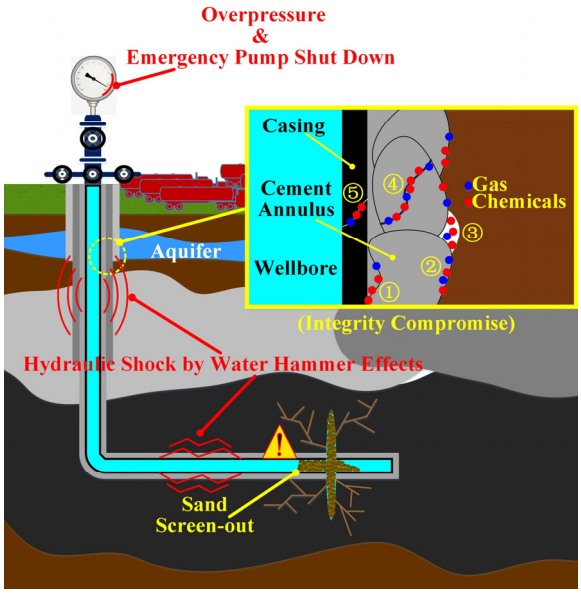

Figure 1. Mechanical mechanisms of well-integrity failure by sand screen-out. The over-injected proppant blocks the formation and wellbore, induces overpressures up-well, and then requires instant pump shut-in, which may cause severe vibrations that damage the cement around casings, as well as the seals between interfaces.

The damage caused by the water-hammer effect on pipes has been demonstrated by sufficient fundamental studies [25,26]. In the oil and gas industry, previous research regarding water-hammer effects mainly focused on the sand production issue in wellbores. The emergency shut-in of injection wells may induce large pressure pulses that can cause wellbore integrity problems, such as sand-face failure and sand production [27,28]. This issue has drawn more concerns in offshore wells, where a higher safety criterion is required for platforms and facilities above sea [29,30]. Recent studies have extended research to the tubing string vibration in high-pressure and high-production gas wells. A numerical simulation showed that a severe stress concentration (895.29 MPa) may be generated in a high-pressure gas well (118 MPa) at the rounded corners of each indentation [19]. The most direct way to control the water-hammer effect is to extend the shut-in time or prevent the rapid shut-in of the gas well [31]. However, this effect during hydraulic fracturing operations and well integrity remains unclear, especially in emergency situations in which an instant pump-rate shutdown may be required to relieve wellhead pressures.

To mitigate this damage in hydraulic fracturing, a data-driven strategy is proposed by integrating the pre-warning of sand screen-out and pump-rate management in real time in fracturing operations [32]. In this study, four cases of shale gas fracturing are presented, in which the wellhead pressure builds up sharply due to the injection of proppant—the typical sign of sand screen-out. Three of the cases follow the pump-rate-regulation strategy (a form of stepwise pump-rate regulation that relieves the seriousness of screen-out with the help of advance warning from the PFI curve) and avoid the accident of sand screen-out [32]. Meanwhile, a sand-screen-out case is also presented to make comparisons between the induced water-hammer effects of different pump-rate-regulation strategies. The results indicate that the stepwise pump-rate-regulation strategy can significantly reduce the impulsive pressure. The hydraulic shock and damage to well integrity can then be restrained to mitigate its environmental risks.

2. Methodology

2.1. Integrated Data-Driven Strategy of Real-Time Monitoring and Regulation

The integrated strategy is proposed based on two hypotheses. (i) Determining elements hypotheses: the pump rate, fracture volume/capacity, and proppant accumulation are proposed as the determining elements contributing to screen-out, according to their significance in hydraulic fracturing [33–36]. The mechanism of screen-out is presumed to result from parameter mismatch among the determining elements [37]. (ii) Linear-correlation hypothesis: the development of fracture networks during proppant injection is ignored when manually labeling the original data, based on which the authors assume that the probability of screen-out has a linear relationship with the injected volume of proppant under constant pump rate, and that the PFI (proppant filling index) has a linear correlation with the ratio of injected proppant volume and the total proppant volume when screen-out occurs. A data-driven workflow is built, based on the hypotheses, for real-time monitoring and regulation and the assessment of water-hammer effects, as shown in Figure 2.

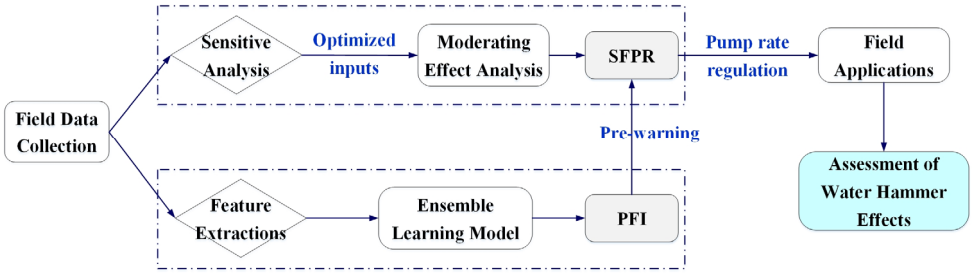

Figure 2. Overall schematic of the integrated data-driven strategy of real-time monitoring and regulation.

According to these hypotheses, the PFI is defined as the volume proportion of proppant-filled fracture in the total volume of proppant-accessible fractures [38]. Subsequently, the PFI based on real-time data on hydraulic fracturing is predicted to monitor the mismatch between proppant supply, by injection, and capacity within the evolving underground fracture network, and therefore presents a continuous time history of risk warnings for fracturing operations. An ensemble learning model was established for predicting the PFI curve for real-time monitoring, as shown in Figure 3a. Meanwhile, the SFPR is defined as the safest fracturing pump rate [37]. The range of SFPR was generated by the prior experiences of screen-out cases learned by a deep learning workflow combined with sensitivity analyses of the U-shaped correlation between pump rate and screen-out probability, as shown in Figure 3b.

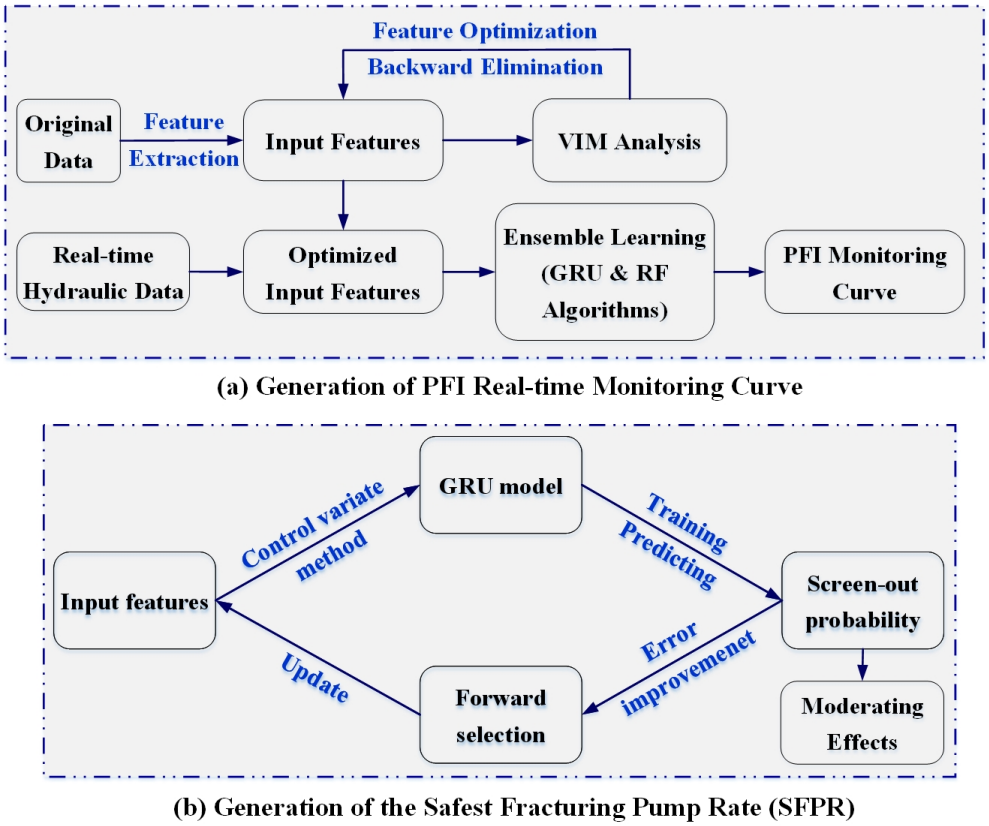

Figure 3. Schematic of data-driven strategy integrating (**a**) PFI and (**b**) SFPR for real-time monitoring and pump-rate regulation [37,38].

Field measurements of shale gas fracturing wells were collected from 18 wells located in the southeast region of the Sichuan Basin, China, which included 29 fracturing stages. These original field parameters involved the geological measurements (well depth, vertical depth, minimum horizontal stress, and pore pressure), well-completion data (stage number and stage length), and hydraulic injection records (pump rate, wellhead pressure, fluid viscosity, proppant diameter, and concentration). These original datasets were pre-processed to extract input features for algorithm training, which is an essential approach in data augmentation. This pre-processing procedure integrates the classical numerical models (as summarized in Section 2.2), and then significantly promotes the performance of algorithms, as observed in our previous study [37].

The Gated Recurrent Unit (GRU) is applied as the core algorithm in the data-processing workflow, as presented in Figure 3. This recurrent neural network is specifically designed to deal with time-series data, such as hydraulic fracturing records during field operations. Two GRU models with 3 layers (including the output layer) were built for predicting PFI and generating SFPR, respectively (as shown in Figure 3). The 'ReLu' was applied as

the activation function in each layer. The Adam routine was selected as the optimizer to compile the model. A callback function was applied to return and automatically update the learning rate, which improves the training efficiency. The grid search and walk-forward validation techniques were combined for the optimization of hyperparameters used for the GRU algorithm. Although the same framework was used, the two GRU models were optimized and trained separately with different training datasets. The PFI is predicted based on both the screen-out and near-screen-out datasets. The SFPR is generated based on the screen-out dataset only. Details of the hyperparameter optimizations and algorithm training are reported in the appendix of our previous study [32]. In this study, we used the well-trained algorithm (for PFI prediction) and SFPR strategy in field trials, and then evaluated the water-hammer effects induced by pump-rate regulations. The SFPR was suggested to be between 5 and 10 m^3/min and to be regulated mildly, based on the collected field data.

2.2. Summary of Numerical Models for Feature Extractions

Both the original parameters and the extracted features were used as the inputs for algorithm training and predictions, as listed in Table 1. The original features included well and vertical depths, minimum horizontal stress, pore pressure, stage number and length, and hydraulic records (pump rate, wellhead pressure, fluid viscosity, and proppant parameters). The extracted features improved the performance of the algorithm significantly by reducing the data noise and estimating the underground situations, which included the volume ratio of injected sand and fluid (V_s/V_f), the wellhead-pressure change in a unit volume of injected fluid ($\Delta P/\Delta V_f$), the downhole pressure after hole perforation (*DPP*), the height of the slurry flowing layer in fractures (H_1), and the fluid efficiency in fractures (η), as presented in Table 1.

Table 1. Summary of original and extracted features for algorithm training.

Original Features	Extracted Features
well depth; vertical depth;	*DPP*
minimum horizontal stress; pore pressure	H_1
stage number; stage length	η
pump rate; wellhead pressure	$\Delta P/\Delta Vf$
fluid viscosity; proppant diameter and concentration	*Vs/Vf*

For the data-noise reduction, the frictions along the injecting pipelines and perforation holes are estimated, and then removed from the wellhead pressure to obtain the downhole pressure after hole perforation (*DPP*)—the fracture inlets. The calculation of *DPP* is given by

$$DPP = P_{wellhead} + P_{statics} - P_{pipeloss} - P_{perforation} \quad (1)$$

The hydrostatic pressure ($P_{statics}$) is calculated from the vertical well depth (h_v)

$$P_{statics} = \rho_s g h_v \quad (2)$$

The frictions along the wellbore ($P_{pipeloss}$) and through the perforations ($P_{perforation}$) are estimated as follows [39]:

$$\begin{cases} P_{pipeloss} = 2f\frac{\rho_s {v_s}^2 L}{h_v} & f = 0.046\left(\frac{\rho_s v_s h_v}{\mu_s}\right)^{-0.2} \\ P_{perforation} = \frac{2.233\times10^{-4} Q^2 \rho_s}{n^2 {d_h}^4 {C_p}^2} \end{cases} \quad (3)$$

where ρ_s is the density of the pumped slurry, kg/m^3; L is the wellbore length from wellhead to the fracturing stage, m; v_s is the flow rate of slurry within the wellbore, m/s; μ_s is the

slurry viscosity, Pa·s; d_h is the diameter of the perforation hole, m; C_p is the coefficient of discharge, and is 0.6–0.95 for slurry; n is the number of the open perforation holes. According to the mini-fracturing tests in fields, typically, approximately half of the designed perforation holes are believed to be open based on the post-mini-fracturing analyses. Due to the lack of direct underground measurements (i.e., the fiber optic distributed acoustic sensing), the number of open perforation holes is assumed to be half of the designed number of perforation holes in this study.

The slurry viscosity (μ_s) is calculated as follows [40]:

$$\mu_s = \mu_f[\frac{5}{2}C_m A^{-1} + (0.32 + \frac{0.38}{1 + 5 \times 10^{-5} A^{-2}})A^{-2}] \qquad A = \frac{C_m}{C} - 1 \tag{4}$$

where C_m is the maximum proppant concentration and is assigned a value of 0.585.

For the underground condition estimations, the proppant dune accumulation (H_1) and fluid efficiency (η) are applied to represent the hydraulic (proppant transport in underground fractures) and rock mechanic (fracture propagations by evaluating the fluids remaining within fractures) features. The bi-power law correlations are proposed to directly calculate the height of the flowing channel (H_1), which is given by [41]

$$\frac{H_1}{w} = [-0.00023\ln(R_G) + 0.00292]R_f^{1.2-0.00126\lambda^{-0.428}[15.2-\ln(R_G)]}R_P^{[-0.0172\ln(R_G)-0.12]} \tag{5}$$

where R_f, R_p, R_G, and λ are calculated by

$$\begin{cases} R_f = \frac{\rho_f Q_f}{w\mu_f} & R_p = \frac{\rho_p Q_p}{w\mu_f} \\ R_G = \frac{\rho_f(\rho_p - \rho_f)gd^3}{{\mu_f}^2} & \lambda = \frac{\mu_f/\rho_f}{w^{1.5}\sqrt{g}} \end{cases} \tag{6}$$

where Q_f is the pump rate of the fracturing fluid, m^3/s; Q_p is the pump rate of the proppant, m^3/s; ρ_p and ρ_f are densities of proppant and fracturing fluid, respectively, in kg/m^3; μ_f is the fluid viscosity, Pa·s; d is the averaged diameter of the proppant, m; and w is the fracture width, m. The fracture width is the only unknown parameter that is presumably set to a value of $50 \times d_{max}$ (d_{max} is the largest diameter of injected proppant), referring to the result from slant-core drilling through a stimulated shale reservoir [42] and numerical simulations [43].

When pure fluid is injected (alternative injection of proppant and pure fluid), the injection of pure fluid may rebalance the proppant dune, which may be calculated from [44]

$$H_1' = H_1 - H_{ridge} = (1 - \frac{2S - 0.1}{7S - 0.05})H_1 \tag{7}$$

where S is the Shields number, and is calculated as

$$S = \frac{8\mu_f Q_f}{(\rho_p - \rho_f)gdw^2 H_1} \tag{8}$$

The fluid efficiency is defined as follows [45,46]:

$$\begin{aligned} \eta &= \eta'(1 - f_{V_p}) + f_{V_p} \\ \eta' &= \frac{V_f}{(V_f + V_l)} \end{aligned} \tag{9}$$

where η is the fluid efficiency; V_f and V_l are the fluid volumes both within the fracture and leaked off, respectively; and f_{Vp} is the volume fraction of proppant in the injected slurry (the ratio of proppant and slurry volumes). Thus, η' is calculated as

$$\begin{array}{l} \left\{ \begin{array}{l} \eta' = \frac{-b-\sqrt{b^2-4ac}}{2a} \\ a = g_l^d - g_u^d \qquad b = g_u^d - 2g_l^d \qquad c = g_l^d - 1 \end{array} \right. \\ \text{where} \\ g^d = g_c / g_0 \\ g_0 = \left[\begin{array}{ll} 4/3 & upper \\ \pi/2 & lower \end{array} \right] \\ g_c = \left[\begin{array}{ll} \frac{4}{3}[(1+\frac{t_c}{t_0})^{3/2} - (\frac{t_c}{t_0})^{3/2}] & upper \\ (1+\frac{t_c}{t_0})\sin^{-1}(1+\frac{t_c}{t_0})^{-1/2} + (\frac{t_c}{t_0})^{1/2} & lower \end{array} \right] \end{array} \tag{10}$$

where a, b, c, ${g_l}^d$, and ${g_u}^d$ are procedural parameters; g^d is a function of time and obtained by field-record analysis after pump shut-in; t_0 is pumping time; and t_c is the fracture-closure time—the time between pump shut-in and fracture closure. For the ongoing fracturing operation, the value of t_c is referred to as the closure times of the neighboring wells.

2.3. Numerical Model for Estimating Water Hammer Effects

The pressure surge caused by water-hammer effects can be estimated by the Joukowsky equation [47]:

$$\Delta P = \rho_f a_w \Delta v \tag{11}$$

where ΔP is the pressure rise due to water-hammer effects, Pa; a_w is the velocity of the pressure impulse wavetrain, m/s; and Δv is the velocity change in the wellbore, m/s.

The velocity of the impulse is calculated as follows [48]:

$$a_w = \sqrt{\frac{1}{\rho_f(\frac{1}{K} + \frac{D}{Ee})}} \tag{12}$$

where K is the bulk module of the liquid, Pa; D is the diameter of the wellbore, m; E is the elasticity modulus of the pipe material, Pa; e is the thickness of the pipe wall, m.

The period of the impulse wave is obtained by dividing the well depth by the velocity of the impulse wave. The steady-state friction expending the pressure surge is estimated from the Darcy–Weisbach equation [49]:

$$P_{friction} = f_r \frac{\rho_f}{2} \frac{\Delta Q^2}{gDA^2} L \tag{13}$$

where f_r is the friction coefficient; g is gravitational acceleration, m/s^2; A is the sectional area of the wellbore, m^2; and ΔQ is the pump-rate change, m^3/s. The friction coefficient is estimated by the Blasius-type friction equation [50]:

$$f_r = 0.184(Re)^{-0.2} \quad Re = \frac{\rho_f D a_w}{\mu_f} \tag{14}$$

where Re is the Reynolds number.

3. Results

3.1. Field Trials of Emergency Pump-Rate Regulations

Three field cases are presented to deploy the PFI monitoring and SFPR regulation, as shown in Figure 4. The deep analyses of the PFI evolutions are explained in our previous study [32]. Generally, the sign of sand screen-out (encountering rapid or vertical increases in wellhead pressures and PFI curves) emerged in the three cases. A stepwise strategy

for pump-rate regulation was applied to reduce the pump rate down to the range of the SFPR (between 5 and 10 m^3/min), as shown in Figure 4. In Case A, the pump rate was reduced stepwise from 18 m^3/min down to 8 m^3/min, and then a pump rate of 10 m^3/min was re-established for the following injection (Figure 4a). In Case B, the pump rate was reduced to 2 m^3/min to terminate the fracturing operation (Figure 4b). In Case C, the pump rate was reduced and then maintained at ~12 m^3/min because of the high proppant concentration and long stage of proppant slug, requiring a relatively high pump rate for the proppant transport. The pressure also decreased at ~12 m^3/min and remained safe when the pump rate was rebuilt up to ~14 m^3/min (Figure 4c).

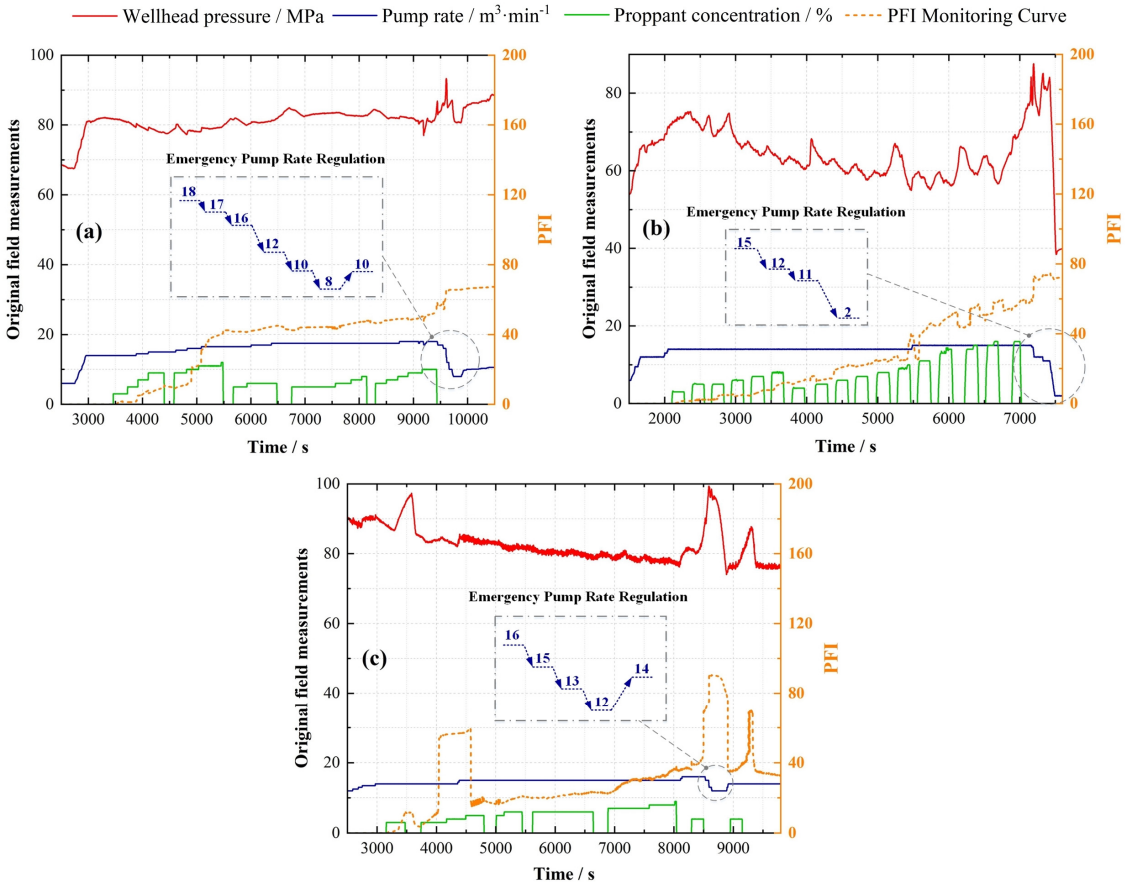

Figure 4. Field trials applying the emergency pump-rate-regulation strategy in (**a**) Case A, (**b**) Case B, and (**c**) Case C. The dashed circles and connected dash–dotted rectangles represent the local amplification of pump-rate regulation, referring to the SFPR [32].

3.2. Field Case of Sand Screen-Out

Case D is a failed example of screen-out prevention, in which the pump rate was sharply reduced and a serious screen-out incident occurred [32], as shown in Figure 5. The PFI reported three vertical jumps during the first three long-duration slugs of proppant injection, as labeled by the three gray dotted–dashed lines in Figure 5a. After the second jump at ~6700 s, the PFI approached 60 in the middle of the fracturing operation, indicating a high proportion of proppant filling in the subsurface fractures. The wellhead pressure, however, registered a slight decrease during the first half of the operation, which is deceptive. The drop in wellhead pressure and the near-continuous rate of proppant injection encouraged the operator to ignore the warning of the PFI, even though it exceeded 80 after 9500 s (Figure 5a). However, the pressure increased sharply soon after the proppant injection. The pump rate was then halved from 16 to 8 m^3/min and, shortly afterward, it was quartered, as shown in Figure 5b. The final slashing of the pump rate to 2 m^3/min may have deteriorated the sand screen-out by promoting the proppant settling. The operators

attempted to boost the pump rate to 4 m^3/min, but encountered a more serious degree of overpressure, indicating a typical screen-out incident. An emergency pump shutdown was executed, with a risk posed to the well integrity from the water-hummer effect. The fracturing operation was suspended in order to open the well, release the pressure, and clean the proppant that flowed back into the well from the fracture.

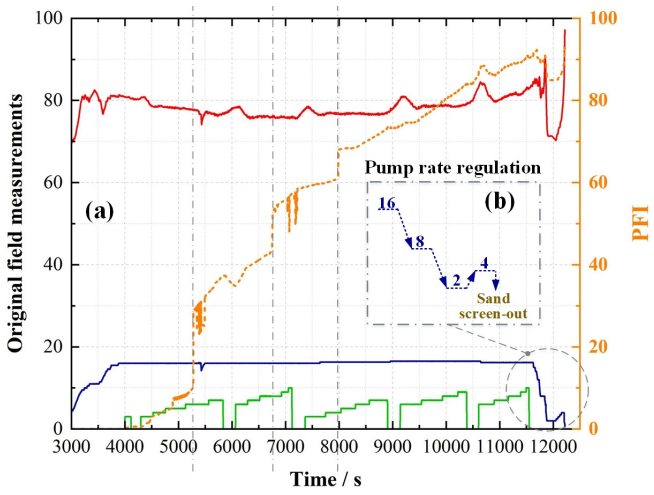

Figure 5. Field records of sand screen-out (**a**) and emergency pump-rate shutdown (**b**) [32].

The reason for the screen-out in Case D may have been the rate of proppant injection (the duration of the injection of the slurry slug, the green curves at the bottom) exceeding the rate of fracture propagation, as reflected in the PFI evolution in Figure 5a. The incident might have been avoided if the operators had slowed down the proppant injection and used shorter slurry slugs after the first PFI jump at ~5000 s in Figure 5a. Therefore, the operator is alerted if the PFI exceeds 50% in the middle of the proppant injection, indicating that the proppant-injection rate may surpass the rate of fracture propagation.

3.3. Impulsive Pressures from Water-Hammer Effect

A rapid change in pump rate may generate a pressure surge (water hammer effect), which can vibrate and damage the casing, thus threatening well integrity. The pressure rise due to pump-rate regulation in Figures 4 and 5 was estimated using the Joukowsky equation (Equation (11)) [47]. This pressure transient propagates along the tube, and its severity is amplified by rapid changes in pump rate, which, in turn, can produce cavitation (bubble production and collapse due to extreme pressure reduction in the tails of the pressure wave) [48,51]. The damping period can be obtained from the ratio of the well depth to the impulse-wave velocity. Wellhead-pressure records intrinsically contain such influences. The peak water-hammer pressure can be recovered from the Darcy–Weisbach equation considering only the steady-state friction (Equation (13)) [49]. Representative magnitudes of the contributing parameters for estimating the impulsive pressure are summarized in Table 2.

Table 2. Summary of parameters for estimating impulsive pressures from water-hammer effects.

Parameters	Values	Parameters	Values
Fluid Density (ρ)	1000 kg/m^3	Diameter of Wellbore (D)	0.127 m
Bulk Module of Liquid (K)	2.2 × 10^9 Pa	Thickness of Pipe Wall (e)	0.0123 m
Elasticity Modulus of Pipe Material (E)	2.0 × 10^{11} Pa	Fluid Viscosity (μ)	0.001 Pa·s
Well Depth (L)	3793 m (Case 1); 3782 m (Case 2); 5252 m (Case 3); 4482 m (Case 4)		

The rough estimations of impulsive pressure induced by the pump-rate regulations are presented in Figure 6, in which the pump-rate changes in Figures 4 and 5 (labeled by dashed circles) are magnified. Generally, a smaller change in the pump rate induces a lower pressure transient. The maximum impulsive pressure (~7.4 MPa) in Cases A~C is restricted and only half of the value in the screen-out case, reaching 14.7 MPa in Case D (Figure 6d). The corresponding frictional resistance to flow in Case D also increases with the increasing velocity of the impulse, resulting in a more rapid attenuation in pressure. Case D presents a mild condition of sand screen-out when the pump rate is successfully reestablished. In more urgent situations, the pressure may continue to increase, even with a reduced pump rate. Therefore, an emergency pump shut-in must be executed, which may cause a pressure rise of 32 MPa (pump shut-in from 12 m^3/min) and result in a reduction in the safety factor of breaching the casing compared with the industry standard [52]. The pressure surge may cause the stress concentrations to exceed the capacity of the casings. Additionally, cyclic loading due to reflections of the pressure wave from the wellbore base and collar may further induce fatigue fractures in both the casing and the cement sheath [19,25].

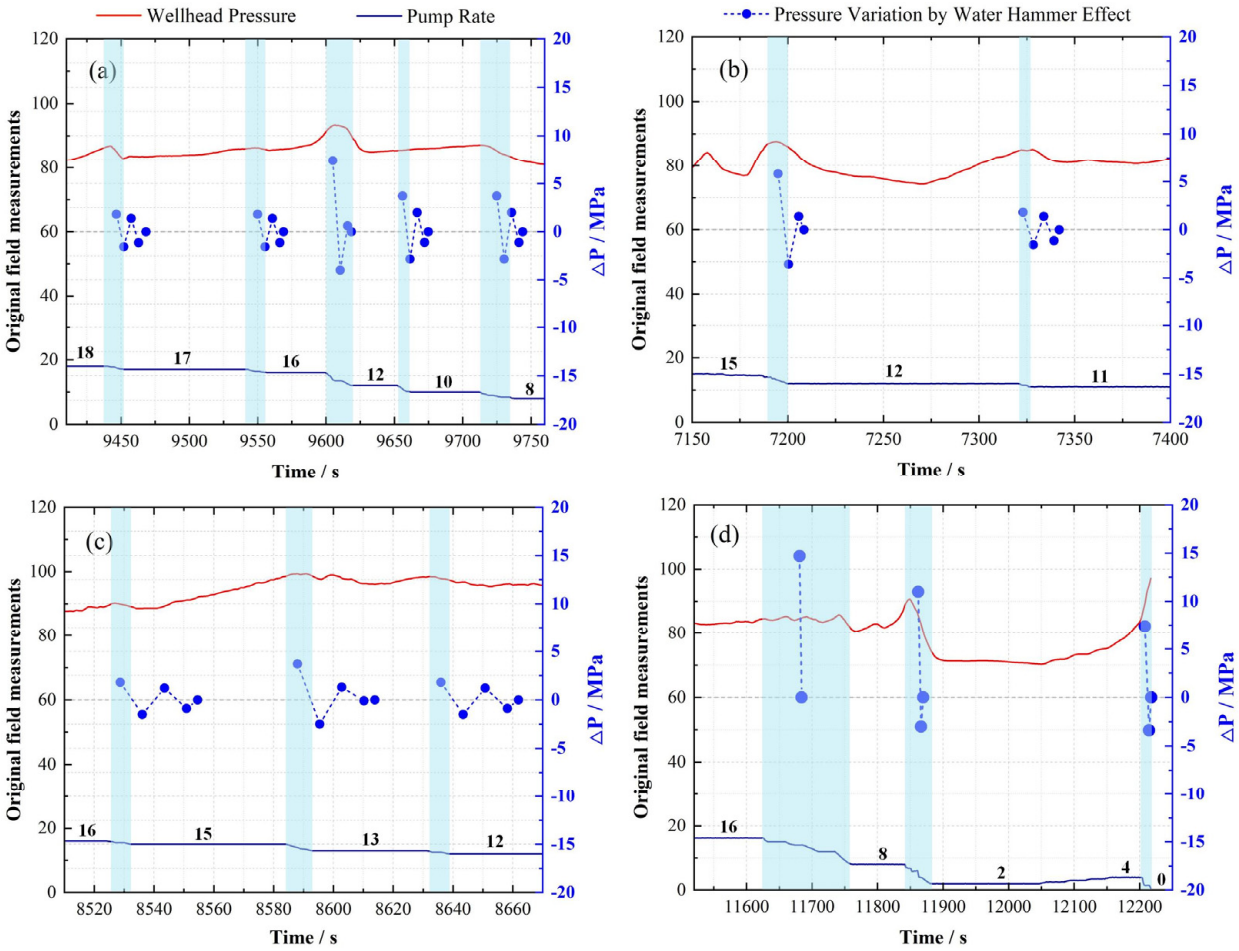

Figure 6. The estimated impulsive pressures from water-hammer effects in (**a**) Case A, (**b**) Case B, (**c**) Case C, and (**d**) Case D. Numbers above the navy curve on the bottom denote values of pump rate. The scattering dash-point curve in the middle is the pressure surge and variations by water-hammer effects.

4. Discussions

4.1. Performance of the Data-Driven Strategy

The performance of the data-driven strategy (combining PFI monitoring and SFPR regulations) is demonstrated by comprehensively analyzing the successful cases (Cases A, B and C) in Figure 4 and the negative case (Case D) in Figure 5. The successful applications

of the SFPR regulation strategy in Cases A, B, and C mitigate the rapid increase in wellhead pressure, which reduces the loss that may be induced by the sand screen-out. Moreover, the PFI curve reports high-value warnings under the condition that the wellhead pressure shows a decreasing trend. Therefore, the presence of the PFI curve provides essential monitoring for field operators to secure fracturing injections. In the middle of the fracturing operation in Case D, the PFI approached a high level of 70 at around 8000 s. This is considered as a valuable warning, 4000 s ahead of the occurrence of sand screen-out, at around 12,000 s, which may spare sufficient time for field operators to perform real-time judgments and adjustments. Moreover, the maximum impulsive pressure (~7.4 MPa) in the SFPR-applied cases (Cases A~C) was significantly reduced, compared with the value (~14.7 MPa) in the sand screen-out in Case 4, in which an emergency pump shut-in was performed. Combined with the pre-warning of the PFI, the pump rate may be regulated gradually to mitigate the reduction amplitude and avoid instant shut-in. These findings agree with the previous results in high-production gas wells, based on which extending the shut-in time was suggested to control the water-hammer effects [31].

4.2. Limitations and Implications

Notably, the stepwise pump-rate-regulation strategy is recommended to be deployed with the PFI real-time monitoring technique. The evolution of the real-time PFI curve reveals the mismatch between the proppant injection and the underground fracture propagation, which provides an important reference to the likelihood of encountering sand screen-out. Moreover, this continuous monitoring allows more reaction time for field operators to make decisions and perform pump-rate regulations. Above all, an instant pump shutdown is mandatory if the wellhead pressure approaches the maximum bearing capacity, in order to secure the humans and equipment around the operation site.

In this study, we used impulsive pressure as the criterion to evaluate the degree of water-hammer effect induced by emergency pump-rate regulations. The real damage to the well integrity by water-hammer effects may be caused by various factors, such as the geological stability of the fracturing formation, the quality of the well cement, and others. A comprehensive evaluation of well integrity or damage by pump-rate regulation is beyond the scope of this study. However, the magnitude of the estimated impulsive pressure can be useful for a comprehensive study. Moreover, the case study in this work demonstrates stepwise pump-rate regulation, which can offer valuable information for the field application of hydraulic fracturing.

5. Conclusions

An integrated data-driven strategy and four field cases of hydraulic fracturing operations were presented to optimize the pump-rate-regulation strategy under the emergency condition of sand screen-out or near sand screen-out. The impulsive pressure induced by the water-hammer effect (due to the pump-rate regulation) was applied as the optimization criterion. By deploying a stepwise pump-rate-regulation strategy, the sand screen-out was successfully prevented in three positive cases. The generated impulsive pressures (3.7~7.4 MPa) were only half or one-third of the pressure (~14.7 MPa) induced by the negative case, in which a more radical regulation strategy was deployed. An instant pump-rate shut-in (for instance, from 12 m^3/min) may further aggravate the impulsive pressure (rise of 32 MPa) and, consequently, threaten the well's integrity. Therefore, the success in applying the integrated data-driven strategy and the stepwise pump-rate-regulation method provides a significant approach to both securing fracturing operations and enhancing well-completion integrity for environmental requirements.

Author Contributions: L.H.: conceptualization, funding acquisition, writing—original draft, investigation; P.G.: data collection, resources, investigation; H.S.: methodology, supervision, software; L.Z.: funding acquisition, methodology, writing—review & editing; J.R.: data curation, resources, writing—review & editing; Y.C.: data curation, resources, writing—review & editing. All authors have read and agreed to the published version of the manuscript.

Funding: This research is funded by the National Natural Science Foundation of China, under the grant 42377138.

Data Availability Statement: The training dataset for algorithm training were used under license for the current study only. The data presented in this study (in figures and tables) are available on request from the corresponding author (due to permission restriction).

Conflicts of Interest: Author Peibin Gong was employed by the Shengli Oilfield Service Corporation. Authors Jianhua Ren and Yiyan Cheng were employed by the East China Company of SINOPEC. The remaining authors declare that the research was conducted in the absence of any commercial or financial relationships that could be construed as a potential conflict of interest.

References

1. Zhai, G.; Shirzaei, M.; Manga, M.; Chen, X. Pore-pressure diffusion, enhanced by poroelastic stresses, controls induced seismicity in Oklahoma. *Proc. Natl. Acad. Sci. USA* **2019**, *116*, 16228–16233. [CrossRef]
2. Schultz, R.; Atkinson, G.; Eaton, D.W.; Gu, Y.J.; Kao, H. Hydraulic fracturing volume is associated with induced earthquake productivity in the Duvernay play. *Science* **2018**, *359*, 304–308. [CrossRef]
3. Howarth, R.W.; Ingraffea, A.; Engelder, T. Should fracking stop? *Nature* **2011**, *477*, 271–275. [CrossRef]
4. Osborn, S.G.; Vengosh, A.; Warner, N.R.; Jackson, R.B. Methane contamination of drinking water accompanying gas-well drilling and hydraulic fracturing. *Proc. Natl. Acad. Sci. USA* **2011**, *108*, 8172–8176. [CrossRef]
5. Vidic, R.D.; Brantley, S.L.; Vandenbossche, J.M.; Yoxtheimer, D.; Abad, J.D. Impact of shale gas development on regional water quality. *Science* **2013**, *340*, 1235009. [CrossRef] [PubMed]
6. Vengosh, A.; Jackson, R.B.; Warner, N.; Darrah, T.H.; Kondash, A. A critical review of the risks to water resources from unconventional shale gas development and hydraulic fracturing in the United States. *Environ. Sci. Technol.* **2014**, *48*, 8334–8348. [CrossRef] [PubMed]
7. Allen, D.T.; Torres, V.M.; Thomas, J.; Sullivan, D.W.; Harrison, M.; Hendler, A.; Herndon, S.C.; Kolb, C.E.; Fraser, M.P.; Hill, A.D.; et al. Measurements of methane emissions at natural gas production sites in the United States. *Proc. Natl. Acad. Sci. USA* **2013**, *110*, 17768–17773. [CrossRef] [PubMed]
8. Warner, N.R.; Jackson, R.B.; Darrah, T.H.; Osborn, S.G.; Down, A.; Zhao, K.; White, A.; Vengosh, A. Geochemical evidence for possible natural migration of Marcellus Formation brine to shallow aquifers in Pennsylvania. *Proc. Natl. Acad. Sci. USA* **2012**, *109*, 11961–11966. [CrossRef] [PubMed]
9. Jackson, R.B.; Vengosh, A.; Darrah, T.H.; Warner, N.R.; Down, A.; Poreda, R.J.; Osborn, S.G.; Zhao, K.; Karr, J.D. Increased stray gas abundance in a subset of drinking water wells near Marcellus shale gas extraction. *Proc. Natl. Acad. Sci. USA* **2013**, *110*, 11250–11255. [CrossRef]
10. Darrah, T.H.; Vengosh, A.; Jackson, R.B.; Warner, N.R.; Poreda, R.J. Noble gases identify the mechanisms of fugitive gas contamination in drinking-water wells overlying the Marcellus and Barnett Shales. *Proc. Natl. Acad. Sci. USA* **2014**, *111*, 14076–14081. [CrossRef]
11. Woda, J.; Wen, T.; Oakley, D.; Yoxtheimer, D.; Engelder, T.; Castro, M.C.; Brantley, S.L. Detecting and explaining why aquifers occasionally become degraded near hydraulically fractured shale gas wells. *Proc. Natl. Acad. Sci. USA* **2018**, *115*, 12349–12358. [CrossRef] [PubMed]
12. Llewellyn, G.T.; Dorman, F.; Westland, J.L.; Yoxtheimer, D.; Grieve, P.; Sowers, T.; Humston-Fulmer, E.; Brantley, S.L. Evaluating a groundwater supply contamination incident attributed to Marcellus Shale gas development. *Proc. Natl. Acad. Sci. USA* **2015**, *112*, 6325–6330. [CrossRef]
13. Jasechko, S.; Perrone, D. Hydraulic fracturing near domestic groundwater wells. *Proc. Natl. Acad. Sci. USA* **2017**, *114*, 13138–13143. [CrossRef]
14. Mumford, A.C.; Maloney, K.O.; Akob, D.M.; Nettemann, S.; Proctor, A.; Ditty, J.; Ulsamer, L.; Lookenbill, J.; Cozzarelli, I.M. Shale gas development has limited effects on stream biology and geochemistry in a gradient-based, multiparameter study in Pennsylvania. *Proc. Natl. Acad. Sci. USA* **2020**, *117*, 3670–3677. [CrossRef] [PubMed]
15. Barth-Naftilan, E.; Sohng, J.; Saiers, J.E. Methane in groundwater before, during, and after hydraulic fracturing of the Marcellus Shale. *Proc. Natl. Acad. Sci. USA* **2018**, *115*, 6970–6975. [CrossRef]
16. Sherwood, O.A.; Rogers, J.D.; Lackey, G.; Burke, T.L.; Osborn, S.G.; Ryan, J.N. Groundwater methane in relation to oil and gas development and shallow coal seams in the Denver-Julesburg Basin of Colorado. *Proc. Natl. Acad. Sci. USA* **2016**, *113*, 8391–8396. [CrossRef] [PubMed]
17. U.S. Department of Energy. *Economic and National Security Impacts under a Hydraulic Fracturing Ban*; U.S. Department of Energy: Wshington, DC, USA, 2021.
18. Office of Governor. Governor Newsom Takes Action to Phase Out Oil Extraction in California. 2021. Available online: https://www.gov.ca.gov/2021/04/23/governor-newsom-takes-action-to-phase-out-oil-extraction-in-california/ (accessed on 17 January 2024).
19. Mou, Y.; Lian, Z.; Sang, P.; Yu, H.; Zhang, Q.; Li, R. Study on water hammer effect on defective tubing failure in high pressure deep gas well. *Eng. Fail. Anal.* **2019**, *106*, 104154. [CrossRef]

20. Zhang, Z.; Wang, J.; Luo, M.; Li, Y.; Zhang, W.; Wu, J.; Li, W. Effect of instantaneous shut-in on well bore integrity and safety of gas wells. *J. Pet. Sci. Eng.* **2020**, *193*, 107323. [CrossRef]
21. Yan, W.; Zou, L.; Li, H.; Deng, J.; Ge, H.; Wang, H. Investigation of casing deformation during hydraulic fracturing in high geo-stress shale gas play. *J. Pet. Sci. Eng.* **2017**, *150*, 22–29. [CrossRef]
22. Hou, L.; Zhang, S.; Elsworth, D.; Liu, H.; Sun, B.; Geng, X. Review of fundamental studies of CO_2 fracturing: Fracture propagation, propping and permeating. *J. Pet. Sci. Eng.* **2021**, *205*, 108823. [CrossRef]
23. Xi, Y.; Lian, W.; Fan, L.; Tao, Q.; Guo, X. Research and engineering application of pre-stressed cementing technology for preventing micro-annulus caused by cyclic loading-unloading in deep shale gas horizontal wells. *J. Pet. Sci. Eng.* **2021**, *200*, 108359. [CrossRef]
24. Holloway, M.D.; Rudd, O. *Fracking: The Operations and Environmental Consequences of Hydraulic Fracturing*; John Wiley & Sons, Incorporated: Hoboken, NJ, USA, 2013.
25. Schmitt, C.; Pluvinage, G.; Hadj-Taieb, E.; Akid, R. Water pipeline failure due to water hammer effects. *Fatigue Fract. Eng. Mater. Struct.* **2006**, *29*, 1075–1082. [CrossRef]
26. Achitaev, A.; Ilyushin, P.; Suslov, K.; Kobyletski, S. Dynamic Simulation of Starting and Emergency Conditions of a Hydraulic Unit Based on a Francis Turbine. *Energies* **2022**, *15*, 8044. [CrossRef]
27. Wang, H.; Hwang, J.; Mukul, M.S. Sand Production Caused by Water Hammer Events: Implications for Shut-In Protocols and Design of Water Injection Wells. In Proceedings of the SPE International Conference and Exhibition on Formation Damage Control, Lafayette, LA, USA, 7–9 February 2018; SPIE: Bellingham, WA, USA, 2018.
28. Tong, Z.; Yang, Z.; Huang, Q.; Yao, Q. Numerical Modeling of the Hydrodynamic Performance of Slanted Axial-Flow Urban Drainage Pumps at Shut-Off Condition. *Energies* **2022**, *15*, 1905. [CrossRef]
29. Tang, Y.; Ouyang, L.-B. A Dynamic Simulation Study of Water Hammer for Offshore Injection Wells To Provide Operation Guidelines. *SPE Prod. Oper.* **2010**, *25*, 509–523. [CrossRef]
30. Choi, S.K.; Huang, W.-S. Impact of Water Hammer in Deep Sea Water Injection Wells. In Proceedings of the SPE Annual Technical Conference and Exhibition, Denver, CO, USA, 30 October–2 November 2011; SPIE: Bellingham, WA, USA, 2011.
31. Zhang, Q.; Liao, T.; Ding, L.; Wang, K.; Yang, H.; Lian, Z. Study on water hammer effect and tubing string vibration in high-pressure high-production gas wells. *Geoenergy Sci. Eng.* **2023**, *229*, 212147. [CrossRef]
32. Hou, L.; Elsworth, D.; Gong, P.; Bian, X.; Zhang, L. Integration of Real-time Monitoring and Data Analytics to Mitigate Sand Screen-outs during Fracturing Operations. *SPE J.* 2024; *revision*.
33. Novotny, E. Proppant transport. In Proceedings of the SPE Annual Fall Technical Conference and Exhibition, Denver, CO, USA, 9–12 October 1977; SPIE: Bellingham, WA, USA, 1977.
34. Patankar, N.A.; Joseph, D.; Wang, J.; Barree, R.; Conway, M.; Asadi, M. Power law correlations for sediment transport in pressure driven channel flows. *Int. J. Multiph. Flow* **2002**, *28*, 1269–1292. [CrossRef]
35. Aud, W.; Wright, T.; Cipolla, C.; Harkrider, J. The effect of viscosity on near-wellbore tortuosity and premature screenouts. In Proceedings of the SPE Annual Technical Conference and Exhibition, New Orleans, LA, USA, 25–28 September 1994; SPIE: Bellingham, WA, USA, 1994.
36. Dahi-Taleghani, A.; Olson, J.E. Numerical modeling of multistranded-hydraulic-fracture propagation: Accounting for the interaction between induced and natural fractures. *SPE J.* **2011**, *16*, 575–581. [CrossRef]
37. Hou, L.; Cheng, Y.; Elsworth, D.; Liu, H.; Ren, J. Prediction of the Continuous Probability of Sand Screenout Based on a Deep Learning Workflow. *SPE J.* **2022**, *27*, 1520–1530. [CrossRef]
38. Hou, L.; Elsworth, D.; Zhang, F.; Wang, Z.; Zhang, J. Evaluation of proppant injection based on a data-driven approach integrating numerical and ensemble learning models. *Energy* **2023**, *264*, 6122. [CrossRef]
39. Willingham, J.; Tan, H.; Norman, L. Perforation friction pressure of fracturing fluid slurries. In Proceedings of the Low Permeability Reservoirs Symposium, Denver, CO, USA, 26–28 April 1993; SPIE: Bellingham, WA, USA, 1993.
40. Dontsov, E.V.; Peirce, A.P. Slurry flow, gravitational settling and a proppant transport model for hydraulic fractures. *J. Fluid Mech.* **2014**, *760*, 567–590. [CrossRef]
41. Wang, J.; Joseph, D.D.; Patankar, N.A.; Conway, M.; Barree, R.D. Bi-power law correlations for sediment transport in pressure driven channel flows. *Int. J. Multiph. Flow* **2003**, *29*, 475–494. [CrossRef]
42. Elliott, S.J.; Gale, J.F.W. Analysis and Distribution of Proppant Recovered From Fracture Faces in the HFTS Slant Core Drilled Through a Stimulated Reservoir. In Proceedings of the 6th Unconventional Resources Technology Conference, Houston, TX, USA, 23 July 2018.
43. Siddhamshetty, P.; Narasingam, A.; Liu, S.; Valkó, P.P.; Kwon, J.S.-I. Feedback control of proppant bank heights during hydraulic fracturing for enhanced productivity in shale formations. In *Computer Aided Chemical Engineering*; Eden, M.R., Ierapetritou, M.G., Towler, G.P., Eds.; Elsevier: Amsterdam, The Netherlands, 2018; Volume 44, pp. 703–708.
44. Hou, L.; Cheng, Y.; Wang, X.; Ren, J.; Geng, X. Effect of slickwater-alternate-slurry injection on proppant transport at field scales: A hybrid approach combining experiments and deep learning. *Energy* **2022**, *242*, 2987. [CrossRef]
45. Nolte, K. A general analysis of fracturing pressure decline with application to three models. *SPE Form. Eval.* **1986**, *1*, 571–583. [CrossRef]
46. Nolte, K. Principles for fracture design based on pressure analysis. *SPE Prod. Eng.* **1988**, *3*, 22–30. [CrossRef]
47. Choon, T.W.; Aik, L.K.; Aik, L.E.; Hin, T.T. Investigation of water hammer effect through pipeline system. *Int. J. Adv. Sci. Eng. Inf. Technol.* **2012**, *2*, 246–251. [CrossRef]

48. Ghidaoui, M.S.; Zhao, M.; McInnis, D.A.; Axworthy, D.H. A review of water hammer theory and practice. *Appl. Mech. Rev.* **2005**, *58*, 49–76. [CrossRef]
49. Bergant, A.; Tijsseling, A.S.; Vítkovský, J.P.; Covas, D.I.; Simpson, A.R.; Lambert, M.F. Parameters affecting water-hammer wave attenuation, shape and timing—Part 1: Mathematical tools. *J. Hydraul. Res.* **2008**, *46*, 373–381. [CrossRef]
50. Siddique, M.; Alhazmy, M. Experimental study of turbulent single-phase flow and heat transfer inside a micro-finned tube. *Int. J. Refrig.* **2008**, *31*, 234–241. [CrossRef]
51. Zhao, L.; Yang, Y.; Wang, T.; Zhou, L.; Li, Y.; Zhang, M. A Simulation Calculation Method of a Water Hammer with Multpoint Collapsing. *Energies* **2020**, *13*, 1103. [CrossRef]
52. Bo, Z.; Yuncai, M.; Yongjin, Z.; Haige, W. Influence of water hammer effect on the well barrier integrity of shale gas well during SRV and the countermeasures. *Oil Drill. Prod. Technol.* **2019**, *41*, 608–613.

Disclaimer/Publisher's Note: The statements, opinions and data contained in all publications are solely those of the individual author(s) and contributor(s) and not of MDPI and/or the editor(s). MDPI and/or the editor(s) disclaim responsibility for any injury to people or property resulting from any ideas, methods, instructions or products referred to in the content.